Theory of Passively Mode-Locked Photonic Crystal Semiconductor Lasers

Heuck, Mikkel; Blaaberg, Søren; Mørk, Jesper

Published in:
Optics Express

Link to article, DOI:
10.1364/OE.18.018003

Publication date:
2010

Document Version
Publisher's PDF, also known as Version of record

Theory of Passively Mode-Locked Photonic Crystal Semiconductor Lasers

Mikkel Heuck, Søren Blaaberg, and Jesper Mørk

DTU Fotonik, Department of Photonics Engineering, Technical University of Denmark, Oersteds Plads 343, DK-2800 Kgs. Lyngby, Denmark

mheu@fotonik.dtu.dk

Abstract: We report the first theoretical investigation of passive mode-locking in photonic crystal mode-locked lasers. Related work has investigated coupled-resonator-optical-waveguide structures in the regime of active mode-locking [Opt. Express **13,** 4539-4553 (2005)]. An extensive numerical investigation of the influence of key parameters of the active sections and the photonic crystal cavity on the laser performance is presented. The results show the possibility of generating stable and high quality pulses in a large parameter region. For optimized dispersion properties of the photonic crystal waveguide cavity, the pulses have sub picosecond widths and are nearly transform limited.

OCIS codes: (140.4050) Mode-locked lasers; (160.5298) Photonic crystals

References and links

1. H. A. Haus and A. Mecozzi, "Noise of mode-locked lasers", IEEE Journal of Quantum Electronics **29,** 983-996 (1993).
2. J. Mulet and J. Mørk, "Analysis of timing jitter in external-cavity mode-locked semiconductor lasers", IEEE Journal of Quantum Electronics **42,** 249-256 (2006).
3. K. Yvind, D. Larsson, L. J. Christiansen, C. Angelo, L. K. Oxenlowe, J. Mørk, D. Birkedal, J. Hvam, and J. Hanberg, "Low-jitter and high-power 40-GHz all-active mode-locked lasers", IEEE Photonics Technology Letters **16,** 975-977 (2004).
4. M. Soljacic and J. D. Joannopoulos, "Enhancement of nonlinear effects using photonic crystals", Nature Materials **3,** 211-219 (2004).
5. E. A. Avrutin, J. H. Marsh, and E. L. Portnoi, "Monolithic and multi-gigahertz mode-locked semiconductor lasers: constructions, experiments, models and applications", IEE Proceedings - Optoelectronics **147,** 251-278 (2000).
6. M. G. Thompson, A. R. Rae, M. Xia, R. V. Penty, and I. H. White, "InGaAs Quantum-Dot Mode-Locked Laser Diodes", IEEE Journal of Selected Topics in Quantum Electronics **15,** 661-672 (2009).
7. R. Hao, E. Cassan, H. Kurt, X. L. Roux, D. Marris-Morini, L. Vivien, H. Wu, Z. Zhou, and X. Zhang, "Novel slow light waveguide with controllable delay-bandwidth product and utra-low dispersion", Optics Express **18**(6), 5942-5950 (2010).
8. J. Li, T. P. White, L. O'Faolain, A. Gomez-Iglesias, and T. F. Krauss, "Systematic design of flat band slow light in photonic crystal waveguides", Optics Express **16**(9), 6227-6232 (2008).
9. A. G. Vladimirov and D. Turaev, "Model for passive mode locking in semiconductor lasers", Physical Review A **72**(3), 033808 (2005).
10. S. Bischoff, M. P. Sørensen, J. Mørk, S. D. Brorson, T. Franck, J. M. Nielsen, and A. M. Larsen, "Pulse-shaping mechanism in colliding-pulse mode-locked laser diodes", Applied Physics Letters **67,** 3877-3879 (1995).
11. A. G. Vladimirov, A. S. Pimenov, and D. Rachinskii, "Numerical Study of Dynamical Regimes in a Monolithic Passively Mode-Locked Semiconductor Laser", IEEE Journal of Quantum Electronics **45,** 462-468 (2009).
12. R. G. M. P. Koumans and R. van Roijen, "Theory for passive mode-locking in semiconductor laser structures including the effects of self-phase modulation, dispersion, and pulse collisions", IEEE Journal of Quantum Electronics **32,** 478-492 (1996).

#127287 - $15.00 USD Received 21 Apr 2010; revised 19 Jul 2010; accepted 19 Jul 2010; published 6 Aug 2010

13. J. Mulet, M. Kroh, and J. Mørk, "Pulse properties of external-cavity mode-locked semiconductor lasers", Optics Express **14,** 1119-1124 (2006).
14. M. D. Settle, R. J. P. Engelen, M. Salib, A. Michaeli, L. Kuipers, and T. F. Krauss, "Flatband slow light in photonic crystals featuring spatial pulse compression and terahertz bandwidth", Optics Express **15,** 219-226 (2007).
15. J. S. Bendat and A. G. Piersol, *Random Data, Analysis and Measurement Procedures*, (John Wiley & Sons, INC., 2000).
16. M. J. R. Heck, E. A. J. M. Bente, Y. Barbarin, D. Lenstra, and M. K. Smit, "Simulation and design of integrated femtosecond passively mode-locked semiconductor ring lasers including integrated passive pulse shaping components", IEEE Journal of Selected Topics in Quantum Electronics **12,** 265-276 (2006).
17. L. A. Coldren and S. W. Corzine, *Diode Lasers and Photonic Integrated Circuits*, (John Wiley & Sons, Inc., 1995).
18. L. H. Frandsen, A. V. Lavrinenko, J. Fage-Pedersen, and P. I. Borel, "Photonic crystal waveguides with semi-slow light and tailored dispersion properties", Optics Express **14,** 9444-9450 (2006).
19. S. Schulz, D. M. Beggs, T. P. White, L. O'Faolain, and T. F. Krauss, "Disorder-induced incoherent scattering losses in photonic crystal waveguides: Bloch mode reshaping, multiple scattering, and breakdown of the Beer-Lambert law", Physical Review B **80**, 195305 (2009).
20. G. P. Agraval, *Nonlinear Fiber Optics*, (Academic Press, 2007).
21. J. A. Leegwater, "Theory of mode-locked semiconductor lasers", IEEE Journal of Quantum Electronics **32,** 1782-1790 (1996).
22. N. Cheng J. C. Cartledge, "Measurement-based model for MQW electroabsorption modulators", Journal of Lightwave Technology **23,** 4265-4269 (2005).

1. Introduction

A mode-locked (ML) laser based on photonic crystal (PC) waveguides (PCW) gives unique possibilities for controlling the pulse properties. Thus, by operating in the slow-light regime, very compact devices can be realized while maintaining a pulse repetition rate compatible with the requirements of optical communication systems. Pulse properties such as the width and chirp can be tuned via the PC dispersion. Also, engineering of the waveguide geometry provides control over the optical density of states, which changes the spontaneous emission and thereby affects the dynamics and noise properties of the laser [1, 2]. High quality monolithic passive mode-locked lasers suitable for optical communication systems have already been demonstrated [3], but for dense integration on photonic chips, the PC structures offer the possibility for the necessary size reduction [4]. Fig. 1 schematically shows the type of structure considered here, where a cavity is created inside the PC structure by removing a line of holes. Mode-locked operation is facilitated by introducing a gain and absorber material in the line defect [5, 6]. Changing the shape and position of holes near the cavity provides vast possibilities for engineering the dispersion. However, it is necessary to perform a detailed investigation of the interplay between the dispersion of the slow-light waveguide and the dynamics of the gain and absorber sections. It is well-known that there is a trade-off between the achievable light slowdown with which the size reduction scales and the bandwidth over which the higher-order dispersion is small [7, 8]. In order to obtain a better understanding of these effects, it is necessary to carefully account for them in a model describing the laser output.

The model that we have developed is described in Section 2, while Section 3 presents the results obtained from numerical solutions of the model equations. In Section 4 the conclusions are summarized.

2. Model

Our model is a modification of that of Vladimirov *et al.* [9], which assumes a ring cavity containing a gain section, an absorber, and a bandwidth limiting filter, see Fig. 2. The dynamics of the carrier density, $N(z,t)$, of the active materials is described by a set of rate equations

$$\partial_t N_r(z,t) = J_r - \gamma_r N_r(z,t) - v_g^b g_r \Gamma_r [N_r(z,t) - N_r^{tr}] |E(z,t)|^2,$$

#127287 - $15.00 USD Received 21 Apr 2010; revised 19 Jul 2010; accepted 19 Jul 2010; published 6 Aug 2010

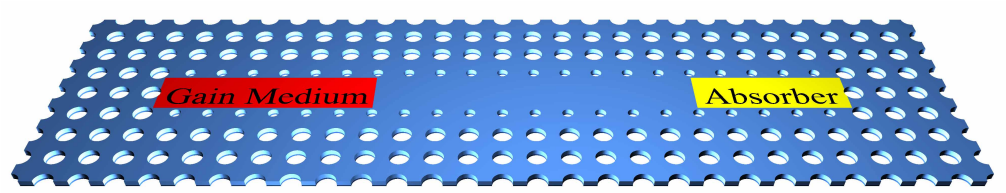

Fig. 1. Illustration of the PC ML laser design. The gain and absorber sections are placed in a line defect cavity, which is created by removing holes of the perfectly periodic PC structure. By altering the shape and position of holes close to the cavity, it is possible to engineer the dispersion properties of the cavity.

for the gain material ($r = g$) and the absorber ($r = q$), respectively. They are coupled to a traveling wave equation for the complex electric field envelope, $E(z,t)$,

$$\partial_z E(z,t) + \frac{1}{v_g^b}\partial_t E(z,t) = \frac{g_r \Gamma_r}{2}(1 - i\alpha_r)[N_r(z,t) - N_r^{tr}]E(z,t). \quad (1)$$

The parameters v_g^b, g_r, Γ_r, and α_r are the group velocity in bulk material, differential gain,

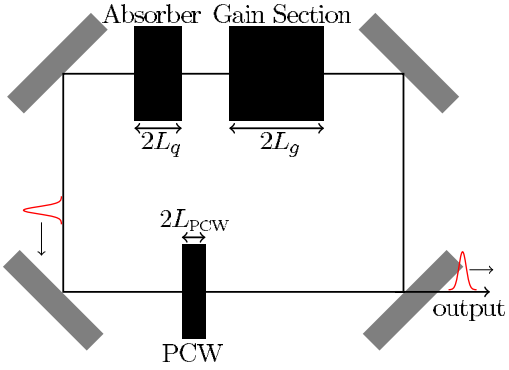

Fig. 2. Illustration of the ring cavity model. The pulse circulates in the cavity, passing through each element.

transverse confinement factor, and line width enhancement factor, respectively. Furthermore, N_r^{tr} is the transparency carrier density, γ_r is the carrier density relaxation rate, J_g is the injected particle current density in the gain material, and for the absorber $J_q = 0$. The use of a reverse biased absorber further means that $\gamma_q \gg \gamma_g$. As seen from Eq. (1), the model assumes a unidirectionally propagating field, which is unable to describe effects such as colliding-pulse mode-locking [10]. This is an essential assumption of our model, since the system under consideration here is a linear cavity, where forwards and backwards propagating waves are expected to play a similar role. However, support for this model is found in [11], where qualitative agreement between bifurcation diagrams showing different solution regimes have been observed for a unidirectional ring cavity model and a model with two counter propagating waves.

Our model is a lumped element model, where the dispersion of the laser cavity and bandwidth limitation of the active sections are treated via a separate component. This approximation is allowed, as long as the effect of the dispersion and bandwidth limitation on the pulse reshaping mechanism is limited [12]. Hence, with the use of a strongly dispersive PCW, this approximation is important to keep in mind.

#127287 - $15.00 USD Received 21 Apr 2010; revised 19 Jul 2010; accepted 19 Jul 2010; published 6 Aug 2010

The pulse widths found in this paper are on the order of 1 ps, where gain nonlinearities such as spectral hole burning and carrier heating start to play a role [13]. Following the model in [9], these effects are, however, not included here. Random spontaneous emission noise [1, 2] is also not considered in this work. The model does not assume small round trip gain or loss as in [12], which makes it suitable for semiconductor active materials.

The transmission of the field through the filter is given by

$$E(z_0, \omega - \omega_0) = \tilde{F}_{\mathrm{PCW}}(\omega - \omega_0) E(z_{\mathrm{PCW}}, \omega - \omega_0)$$

where $\tilde{F}_{\mathrm{PCW}}(\omega - \omega_0)$ is the complex transfer function of the filter. By integrating over the spatial coordinate and using a Lorentzian transfer function, a set of nonlinear coupled delay differential equations can be obtained [9]. In the case considered here, a more general form of the transfer function is used, which provides the necessary freedom to describe the influence of the strong dispersion of the PCW on the laser output

$$\tilde{F}_{\mathrm{PCW}}(\omega - \omega_0) = e^{i\phi(\omega-\omega_0)} f_H(\omega - \omega_0), \quad \tilde{F}_{\mathrm{PCW}}(\omega) = \int_{-\infty}^{+\infty} F_{\mathrm{PCW}}(t) e^{i\omega t} \tag{2}$$

$$\phi(\omega - \omega_0) = \frac{2L_{\mathrm{PCW}}}{2k_0} \left(\left[\sum_{p=0}^{3} \frac{1}{p!} k_{\omega_0}^{(p)} (\omega - \omega_0)^p \right]^2 - k_0^2 \right), \qquad k_{\omega_0}^{(p)} = \left. \frac{d^p k(\omega)}{d\omega^p} \right|_{\omega=\omega_0} \tag{3}$$

$$f_H(\omega - \omega_0) = \sum_{p=1}^{3} |a_p| \exp\left(-b_p^2 \left[(\omega - \omega_0)^2 - c_p^2\right]\right). \tag{4}$$

The expression in Eq. (3) is obtained by considering the passage of the electric field through a homogeneous material with susceptibility $\chi(\omega)$, which is related to the wavenumber by $k^2(\omega) = \omega^2/c^2(1 + \mathrm{Re}\{\chi(\omega)\})$. In Eq. (3) this expression is replaced by the first 4 terms of its Taylor expansion. The dispersion relation, $k(\omega)$, of the PCW is found from a band structure calculation and the parameter values used in this work are chosen using the results of Settle *et al.* [14] as a guideline. The real function $f_H(\omega)$ accounts for the spectral amplitude filtering. All physical transfer functions are subject to a causality condition, which imposes the restriction that $F_{\mathrm{PCW}}(t \leq 0) = 0$. This, in turn, gives rise to the following relation between the real and imaginary parts of $\tilde{F}_{\mathrm{PCW}}(\omega)$ [15]

$$\int_{-\infty}^{+\infty} \frac{f_H(u)\cos[\phi(u)]}{\pi(\omega - u)} du = f_H(\omega)\sin[\phi(\omega)]. \tag{5}$$

Since $\phi(\omega)$ is completely determined by the dispersion relation, $f_H(\omega)$ is determined by Eq. (5). However, the Taylor expansion used in Eq. (3) is only a good approximation within a limited bandwidth, so solving Eq. (5) without any restrictions on $f_H(\omega)$ is not a good approach. For this reason, we have chosen the definition in Eq. (4) with the adjustable parameters $\{a_p, b_p, c_p\}$, where the values of b_p are of course restricted. An iteration approach is used to determine these parameters using Eq. (5). This is done by inserting an initial guess on the LHS and fitting the result of the integral to the form of the RHS. The new parameter values $\{a_p, b_p, c_p\}$ are then reinserted on the LHS and so on. For small values of $k_{\omega_0}^{(3)}$ and large filter bandwidths, the transfer function has a significant value for $t \leq 0$ if a single Gaussian with fixed values of $\{a_1, b_1, c_1\}$ is used. By using Eq. (4) and the iteration procedure described above, it is, however, possible to make F_{PCW} fulfill the causality condition to a far better extent. For the specific parameter values used here, however, it makes no significant difference if a single Gaussian is used for f_H without the iteration procedure. In general, it is important to check the result of the iteration method as there is no guarantee of convergence. The causality condition is not

#127287 - $15.00 USD Received 21 Apr 2010; revised 19 Jul 2010; accepted 19 Jul 2010; published 6 Aug 2010

addressed in the related work of Heck *et al.* [16], where a transfer function approach is also used to describe a passive dispersive element.

With $\tilde{F}_{\mathrm{PCW}}(\omega)$ given by Eq. (2), the resulting model equations are

$$d_\tau G(\tau) = g_0 - \Gamma G(\tau) - e^{-Q(\tau)}\left(e^{G(\tau)}-1\right)|A(\tau)|^2 \tag{6}$$

$$d_\tau Q(\tau) = q_0 - Q(\tau) - s\left(1-e^{-Q(\tau)}\right)|A(\tau)|^2 \tag{7}$$

$$A(\tau) = \int_{-\infty}^{\tau} F_{\mathrm{PCW}}(\tau-u)R(u-T_0)A(u-T_0)du \tag{8}$$

with

$$R(\tau) = \sqrt{\kappa}\exp\left[(1-i\alpha_g)\frac{G(\tau)}{2} - (1-i\alpha_q)\frac{Q(\tau)}{2}\right].$$

The time domain transfer function in Eq. (8) is calculated from Eq. (2) using a numerical Fourier transformation. The normalizations used in Eqs. (6)-(8) are

$$\zeta = \frac{\gamma_q}{v_g^b}z, \qquad \tau = \gamma_q\left(t-\frac{z}{v_g^b}\right), \qquad \Gamma = \frac{\gamma_g}{\gamma_q}, \qquad s = \frac{g_q\Gamma_q}{g_g\Gamma_g}$$

$$A(\zeta,\tau) = E(\zeta,\tau)\sqrt{\frac{v_g^b}{\gamma_q}g_g\Gamma_g}, \qquad A(\tau) = A(\zeta_0,\tau)$$

$$G(\tau) = \int_{z_g}^{z_g+L_g} g_g\Gamma_g[N_g - N_g^{tr}]dz \qquad Q(\tau) = -\int_{z_q}^{z_q+L_q} g_q\Gamma_q[N_q - N_q^{tr}]dz$$

$$g_0 = \int_{z_g}^{z_g+L_g}\left(J_g - \gamma_g N_g^{tr}\right)\frac{g_g\Gamma_g}{\gamma_q}dz \qquad q_0 = \int_{z_q}^{z_q+L_q} N_q^{tr}g_q\Gamma_q dz\,.$$

The round trip non-resonant loss, $\sqrt{\kappa}$, accounts for propagation and mirror losses and $T_0 = \gamma_q/v_g^b(2L_{\mathrm{PCW}}+2L_g+2L_q)$ is the normalized cold cavity round trip time. The length of the gain section (absorber) is $2L_g$ ($2L_q$). The delay term, $u-T_0$, in Eq. (8) arises from the periodic boundary condition of the ring cavity: $E(z+2L_{\mathrm{tot}},t) = E(z,t)$, where $2L_{\mathrm{tot}} = 2L_{\mathrm{PCW}}+2L_g+2L_q$ is the total round trip length of the cavity.

3. Simulation Results

We have solved Eqs. (6)-(8) numerically to investigate how the laser output depends on the parameters. Using the results in [9] as a starting point, we use parameter values that are typical of standard ridge waveguide in-plane quantum well lasers [9, 17]. Unless otherwise stated, we use the parameter values given in Table 1. The output power of the laser is

$$P = t_{out}|E|^2\hbar\omega_0\Gamma_g A_\sigma v_g^b$$

where A_σ is the cross sectional area of the waveguide perpendicular to the z-axis and t_{out} is the output coupling factor. Designs like the one shown in Fig. 1 can have large quality factors resulting in a value of κ much closer to 1 than the one given in Table 1. This, in turn, means that the threshold gain, $g_0^{th} = \Gamma[q_0 - \ln(\kappa)] = 0.014$, becomes smaller and the laser can be driven by smaller pumping currents. The values of the parameters in Eq. (4) are $a_1 = 0.33$, $a_2 = 0.37$, $a_3 = 0.3$, $b_1 = 0.015$, $b_2 = 0.016$, $b_3 = 0.013$, $c_1 = 5.82\times10^{-9}$, $c_2 = 1$, and $c_3 = -1$. With these parameters $f_H(\omega-\omega_0)$ looks like a Gaussian with a FWHM width of 1.25 THz. In Figs. 3-9 the linewidth enhancement factors are zero, and in Fig. 10 an investigation of the effects of changing the α-parameters is presented.

#127287 - $15.00 USD Received 21 Apr 2010; revised 19 Jul 2010; accepted 19 Jul 2010; published 6 Aug 2010

Table 1. Parameter values used unless otherwise stated in the figure captions.

Parameter Values		
$k_0 = 1.42\times10^{7}$ m^{-1}	$L_{\mathrm{PCW}} = 40\ \mu$m	$s = 25$
$k^{(1)}_{\omega_0} = 1.75\times10^{-7}$ sm^{-1}	$A_\sigma = 0.016\times10^{-12}$ m^2	$g_0 = 3.5$
$k^{(2)}_{\omega_0} = 1.86\times10^{6}$ ps^2/km	$\Gamma = 1.33\times10^{-3}$	$q_0 = 8$
$k^{(3)}_{\omega_0} = 0.29\times10^{6}$ ps^3/km	$\Gamma_g = \Gamma_q = 0.032$	$\kappa = 0.1$
$v^b_g = 8.57\times10^{7}$ ms^{-1}	$\gamma_q = 10^{11}$ s^{-1}	$T_0 = 0.14$
$g_g = 5.34\times10^{-20}$ m^2	$L_g = 18.6\ \mu$m	$t_{out} = 0.7$
$N^{tr}_g = 0.9\times10^{24}$ m^{-3}	$L_q = 1.93\ \mu$m	

Phase Diagram

Eqs. (6)-(8) have qualitatively different types of solutions depending on the values of the unsaturated gain, g_0, and loss, q_0. The left plot in Fig. 3 shows a phase diagram of the different solution types. The large size of the green domain representing ML solutions shows that mode locked behavior is not critically dependent on the exact values of g_0 and q_0, which shows promise for an experimental realization of the laser design. The smaller green regions at larger

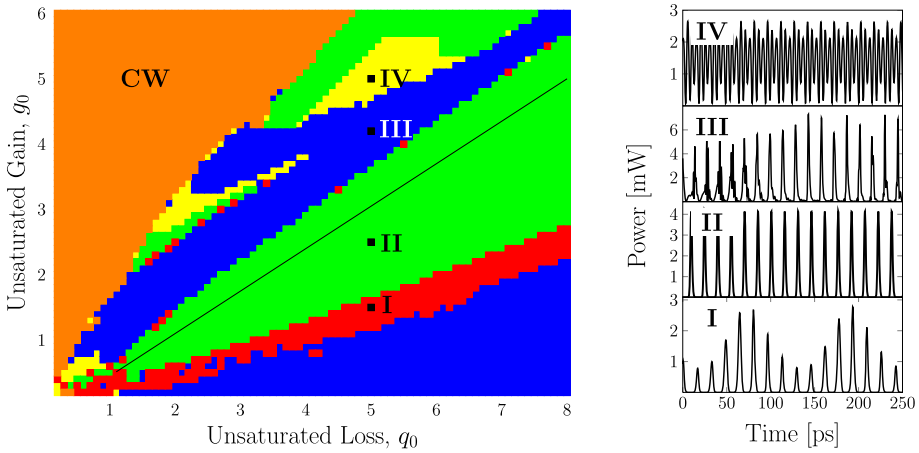

Fig. 3. Left: Phase diagram of possible solution types as a function of the unsaturated gain, g_0, and loss, q_0. The green domain represents ML solutions, red is intensity modulated pulses, blue is irregular solutions with no periodicity, yellow is higher harmonic solutions and orange is CW solutions. Pulse properties of solutions restricted to the black line are shown in Fig. 4. Right: Plots of the different solution types depending on the value of (q_0, g_0). I: $(q_0, g_0) = (5, 1.5)$, II: $(q_0, g_0) = (5, 2.5)$, III: $(q_0, g_0) = (5, 4.2)$, IV: $(q_0, g_0) = (5, 5)$.

ratios of g_0/q_0 correspond to higher harmonic ML regimes with several pulses per round trip time. Solutions in the narrow green region around $(q_0, g_0) = (2.5, 2.5)$ have 2 pulses in each round trip time whereas solutions in the uppermost green region have 3. The relative positions of the different regions in the left plot of Fig. 3 qualitatively agree with FIG. 5 in [9]. Note that the values of g_0 and q_0 in Fig. 3 are very large compared to the transparency value, meaning

#127287 - $15.00 USD Received 21 Apr 2010; revised 19 Jul 2010; accepted 19 Jul 2010; published 6 Aug 2010

that the laser is pumped very hard in this regime.

The graphs in the right plot of Fig. 3 show examples of the different solution types for values of g_0 and q_0 indicated by the location of the corresponding roman numerals in the left plot.

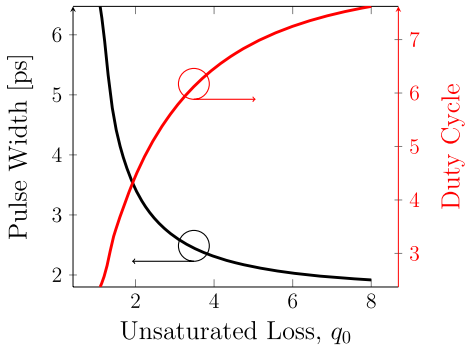

Fig. 4. Variation of the pulse width (black) and duty cycle (red) for (q_0, g_0) restricted to the line $g_0 = 0.65q_0 - 0.2$ in the left plot of Fig. 3.

The variation of the full width at half maximum (FWHM) pulse width, Δt_{FWHM}, and duty cycle, $T/\Delta t_{\mathrm{FWHM}}$, for ($q_0$, g_0) restricted to the black line in the left plot of Fig. 3 is shown in Fig. 4. T is the period of the output pulse train. The pulse width is seen to be large and vary significantly for small values of q_0. The duty cycle expresses how closely the pulses are spaced, and from Fig. 4 it is clear that q_0 must be sufficiently large in order for the pulses to become well separated.

Influence of PC Dispersion

To obtain short pulses it is important to have a large frequency interval over which the dispersion is nearly linear so that broadening of the pulses due to group velocity dispersion (GVD) is minimized. Designs for "semi-slow" light waveguides are therefore of interest [14, 18]. Fig. 5(a) shows a plot of the Taylor expansion of $k(\omega)$ in Eq. (3). The gray region marks the frequency interval, where the group index is approximately constant. For a small filter bandwidth the transform limit sets a lower bound on the achievable pulse width and for a large bandwidth the pulse width is limited by either GVD or the dynamics of the interaction of the field with the active sections. In Fig. 5(b) the dependence of the pulse width and pulse bandwidth, Δf_{FWHM}, on the filter bandwidth, Δf_{PCW}, is depicted. It clearly shows that the pulse width increases significantly as the filter bandwidth becomes small. The ratio $\Delta f_{\mathrm{FWHM}}/\Delta f_{\mathrm{PCW}}$ also becomes large, which indicates that the small filter bandwidth is the cause of the pulse broadening. The flattening of the black curve along with the decrease of $\Delta f_{\mathrm{FWHM}}/\Delta f_{\mathrm{PCW}}$ for large filter bandwidths indicate that in this parameter region, the pulse width is determined by the gain and loss dynamics rather than GVD. The largest filter bandwidth in Fig. 5(b) is smaller than the PCW transmission window and typical gain bandwidths, so it does not correspond to any of the components of the system described in Fig. 1. This bandwidth limitation is however necessary in our model in order for the Taylor expansion in Eq. (3) to be a good approximation. With a filter bandwidth of 1.25 THz, we operate close to the domain where the pulse width is predominantly determined by gain and loss dynamics, and thus it has a limited physical impact that we use a filter bandwidth, which is smaller than the gain bandwidth and the PCW transmission window.

#127287 - $15.00 USD Received 21 Apr 2010; revised 19 Jul 2010; accepted 19 Jul 2010; published 6 Aug 2010

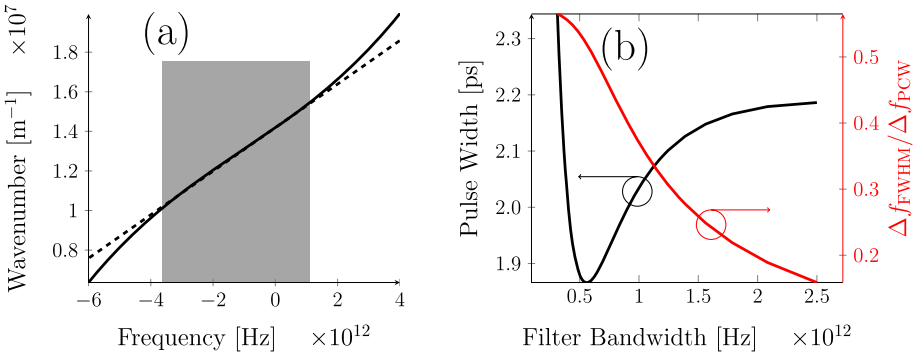

Fig. 5. (a) A plot of the Taylor expansion (solid black) of the dispersion relation with parameter values from Table 1. The group velocity is constant along the dashed black line. The frequencies on the abscissa are $f-\omega_0/2\pi$, were ω_0 is the fast oscillating part of the total field, $\mathscr{E}(z,t)=E(z,t)e^{ik_0z-i\omega_0t}$. (b) Variation of the pulse width in the time (black) and frequency domain (red) with the filter bandwidth, Δf_{PCW}.

Compact Laser Design

By designing the structure shown in Fig. 1 to have a large group index, it is possible to reduce the overall size of the laser. For this reason it is important to understand the influence on the pulse properties of changing the PCW length and the group index. Fig. 6(a) shows the results of simulations with different waveguide lengths, $2L_{\mathrm{PCW}}$. The pulse width is observed to increase linearly for large values of $2L_{\mathrm{PCW}}$, but it gradually starts deviating from this behavior as $2L_{\mathrm{PCW}}$ decreases to 40 μm, where a transition to an irregular solution type occurs. Notice that Δt_{FWHM} varies only 20% when $2L_{\mathrm{PCW}}$ is increased by 250%. The repetition rate, f_r, obtained under cold cavity conditions is

$$f_r=\frac{1}{T}=\left[\frac{1}{v_g^b}\left(S\times 2L_{\mathrm{PCW}}+2L_{\mathrm{tot}}\right)\right]^{-1}. \tag{9}$$

Here, $S=v_g^b/v_g$ is the slowdown factor and v_g is the group velocity in the PCW. The value of f_r obtained from Eq. (9) is plotted in Fig. 6(a) and it is seen to agree well with the repetition rate found from the solution of Eqs. (6)-(8). The small deviation is attributed to pulse reshaping in the active sections, which depends on the pulse energy.

To investigate the effect of reducing the device size by increasing the slowdown factor, we have varied $2L_{\mathrm{PCW}}$ and S simultaneously while keeping their product constant to keep f_r approximately constant. The result is depicted in Fig. 6(b). The repetition rate is 66 GHz and decreases about 5% in the considered interval. The length reduction factor, $\rho_R=\left[(S-1)2L_{\mathrm{PCW}}+2L_{\mathrm{tot}}\right]/2L_{\mathrm{tot}}$, expresses how much smaller the laser can be made compared to a conventional design without the PCW structure if their cold cavity repetition rates are equal. The reason for using $S-1$ in this definition is to ensure that $\rho_R=1$ for $S=1$. There is a difference between this expression and Eq. (9), where the contribution $2L_{\mathrm{PCW}}$ is counted twice. $T_0=(\gamma_q/v_g^b)2L_{\mathrm{tot}}$ has to be the total normalized cold cavity round trip time due to the periodic boundary condition, but the time it takes to pass the PCW is added to T_0 in the model, which results in the term $2L_{\mathrm{PCW}}/v_g^b$ being counted twice in Eq. (9). This does not affect any of the conclusions drawn here, and the issue could be circumvented by replacing $k_{\omega_0}^{(1)}$ with $k_{\omega_0}^{(1)}-1/v_g^b$ in the first order term in Eq. (3). This would subtract the term, which is counted twice in Eq. (9) while maintaining the correct value of $k_{\omega_0}^{(1)}$ in the higher order terms. Another

#127287 - $15.00 USD Received 21 Apr 2010; revised 19 Jul 2010; accepted 19 Jul 2010; published 6 Aug 2010

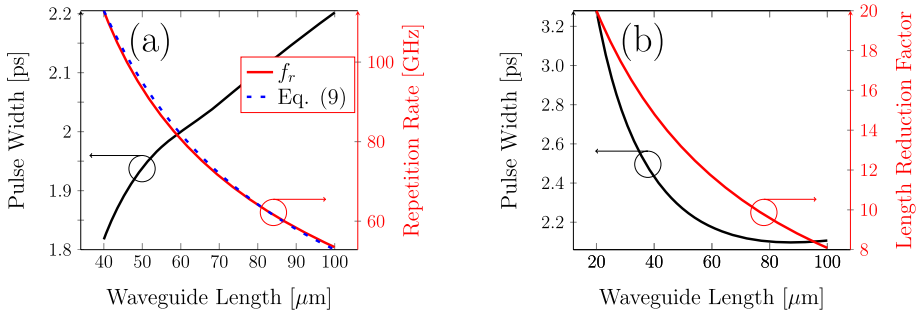

Fig. 6. (a) Variation of the pulse width (black) and the repetition rate, f_r, (red) with the length of the PCW, $2L_{\mathrm{PCW}}$. The dashed blue line shows f_r from Eq. (9). (b) Variation of the pulse width (black) and length reduction factor, ρ_R, (red) as the length of the PCW and the slowdown factor are varied simultaneously, while keeping their product $S \times 2L_{\mathrm{PCW}} = 1200\ \mu$m constant.

issue is that $\rho_R = 20$ when $S = 60$ in Fig. 6(b), but from the design shown in Fig. 1, the length reduction factor is expected to be approximately equal to the slowdown factor since the PCW fills up the entire cavity. By setting $L_g = L_q = 0$ this would indeed be the case, but we keep the

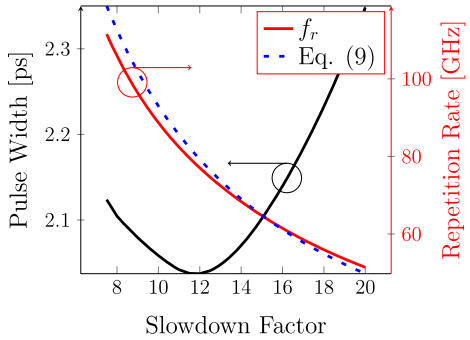

Fig. 7. Variation of the pulse width (black) and repetition rate (red) as a function of the slowdown factor. The dashed blue line shows f_r from Eq. (9).

more general formulation with nonzero lengths and merely note that ρ_R is expected to be larger than the values shown in Fig. 6(b). From Fig. 6(b) it is also seen that the length reduction comes at the price of an increasing pulse width, which varies significantly for small values of $2L_{\mathrm{PCW}}$.

In Fig. 7 the influence of varying only the slowdown factor is investigated. The pulse width is seen to have a minimum, but the overall variation of Δt_{FWHM} is only about 13% indicating that the pulse width is not strongly dependent on S for the parameter values shown here. Fig. 7 also shows that the repetition rate deviates more from Eq. (9) than when varying the cavity length in Fig. 6(a).

When the slow light effect of a PCW is used to reduce the size of a laser structure, the scattering losses due to fabrication imperfections increase with decreasing group velocity [19]. This is an important effect to keep in mind, and it could be implemented in our model by letting κ be a function of the group velocity.

#127287 - $15.00 USD Received 21 Apr 2010; revised 19 Jul 2010; accepted 19 Jul 2010; published 6 Aug 2010

Pulse Distortion

It is important to consider the influence of the strong dispersion of the PCW on the laser output. For large values of $k^{(3)}_{\omega_0}$ the pulse shape is distorted by the formation of trailing pulses, see graph **III** in Fig. 8. The ratio between the peak power of the trailing and main pulse, $P_0^{\text{trailing}}/P_0^{\text{main}}$, is shown in Fig. 9(a) as a function of the second and third order expansion coefficients in Eq. (3). The blue region, where the ratio equals zero, corresponds to solutions

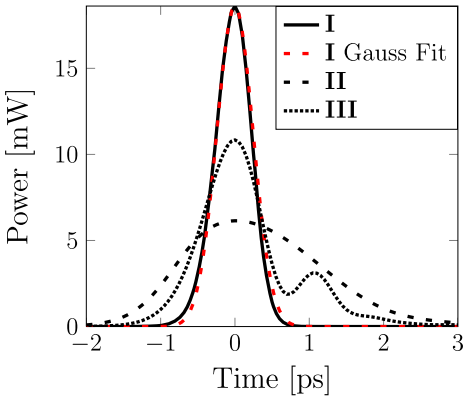

Fig. 8. Pulse shape for different values of the second and third order expansion coefficients in Eq. (3). The values of $(k^{(3)}_{\omega_0}, k^{(2)}_{\omega_0})$ for the different curves are shown in Fig. 9 by the location of the corresponding roman numerals. The dashed red line shows a Gaussian fit to pulse **I**.

with no trailing pulse. Fig. 9(a) shows how the region of distorted pulses expands as $k^{(3)}_{\omega_0}$ increases. The trailing pulse forms from a shoulder on the main pulse, where a dip arises in the field envelope. This occurs at the boundary line between the blue and the triangular shaped region in Fig. 9(a). The closer $k^{(2)}_{\omega_0}$ is to -2.1×10^6 ps^2/km, the more this dip opens due to an increasing lag of the trailing pulse and the ratio decreases while the width of the trailing pulse increases. The symmetry line at $k^{(2)}_{\omega_0} = -2.1\times10^6$ ps^2/km in Fig. 9(a) and 9(b) corresponds to a zero value of the second order term, $[k^{(1)}_{\omega_0}]^2/k_0 + k^{(2)}_{\omega_0}$, in Eq. (3). The approximation $k^2(\omega) - k_0^2 \approx 2k_0[k(\omega) - k_0]$, which is usually made when deriving e.g. the traveling wave equation [20], predicts the symmetry line to be placed at $k^{(2)}_{\omega_0} = 0$. The translation of this line in Fig. 9 shows that this approximation is not valid here due to the large slowdown factor. As mentioned in Section 2, Eq. (3) was derived assuming that $\chi(\omega)$ is position independent, but the values of the expansion coefficients come from a band structure calculation in which $\chi(\omega)$ varies significantly with position.

Fig. 9(b) shows the dependence of the pulse width on the second and third order expansion coefficients in Eq. (3). It is seen that the pulse width reaches the sub picosecond range when $k^{(2)}_{\omega_0}$ is around -2.1×10^6 ps^2/km and from Fig. 9(a) it is evident that $k^{(3)}_{\omega_0}$ can attain large values without significant pulse distortion, when the value of $k^{(2)}_{\omega_0}$ is in this optimum range. Fig. 8 shows plots of the pulse shape for different values of $(k^{(3)}_{\omega_0}, k^{(2)}_{\omega_0})$ indicated by the location of the corresponding roman numerals in Fig. 9. Graph **III** gives an example of a distorted pulse, whereas **II** shows the pulse shape obtained with the parameters found by Settle *et al.* [14]. This case shows no trailing pulses and the values of $k^{(2)}_{\omega_0}$ and $k^{(3)}_{\omega_0}$ lie well within the blue region in Fig. 9(a), again showing promise for realizations. Graph **I** shows a very narrow pulse and the

#127287 - $15.00 USD Received 21 Apr 2010; revised 19 Jul 2010; accepted 19 Jul 2010; published 6 Aug 2010

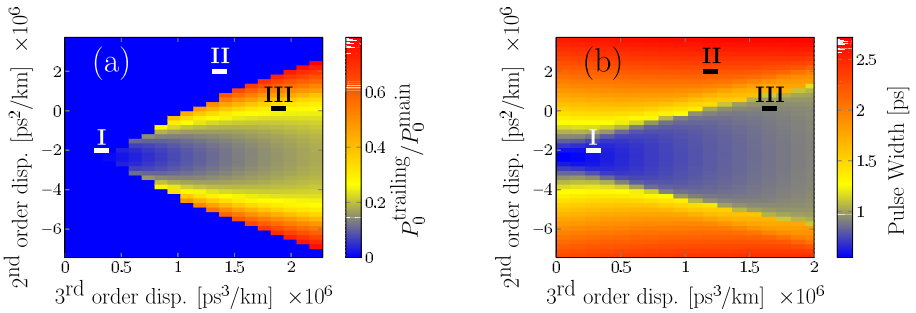

Fig. 9. (a) The dependence of the ratio between the trailing and main pulse peak powers on the second and third order expansion coefficients in Eq. (3). (b) Pulse width as a function of the second and third order expansion coefficients in Eq. (3).

red dashed line shows that the shape is Gaussian to a good approximation. The time-bandwidth product (TBP), $\Delta t_{\text{FWHM}}\Delta f_{\text{FWHM}}$, is very close to the transform limit for Gaussian pulses in the region of small pulse width in Fig. 9(b). It increases by a factor of 2 for the widest pulses, due to pulse broadening induced by the PCW dispersion described by the phase part of Eq. (2).

In Fig. 9 we varied the higher order dispersion coefficients freely, but it is an open question whether all points in this phase space are obtainable by changing the PCW geometry. Investigations of shifting the neighboring rows along [7] and perpendicular to [8] the propagation direction do, however, suggest that the size of the phase space used in Fig. 9 is well within the physically obtainable limits.

Linewidth Enhancement Factors

So far, all the simulations have been performed with the linewidth enhancement factors, α_g and α_q, equal to zero. Since they cause self phase modulation (SPM) of the pulses, it is, however, important to investigate their influence on the laser output. Fig. 10(a) shows a phase diagram of solution types depending on α_q and α_g. The colors refer to the same solution types as in Fig. 3.

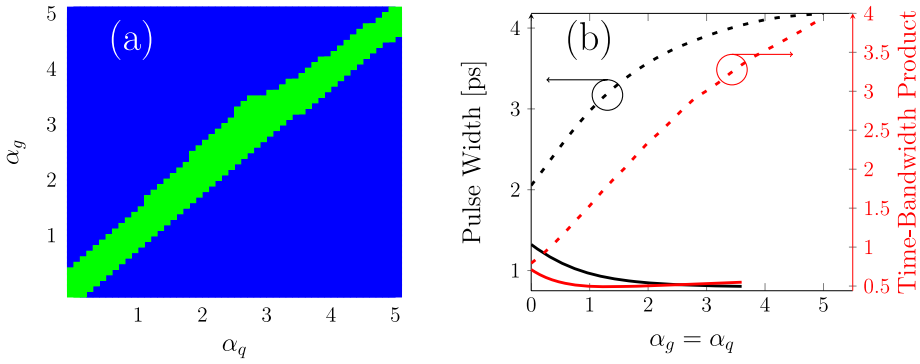

Fig. 10. (a) A phase diagram of solution types found by varying the linewidth enhancement factors. The color code is the same as in Fig. 3. (b) Variation of the pulse width (black) and time-bandwidth product, $\Delta t_{\text{FWHM}}\Delta f_{\text{FWHM}}$, (red) as a function of the linewidth enhancement factors. The values of $[k^{(1)}_{\omega_0}]^2/k_0 + k^{(2)}_{\omega_0}$ are -4×10^6 ps^2/km (dashed lines) and 2×10^6 ps^2/km (solid lines).

It is observed that the range of α-parameters, for which stable ML behavior occurs, is rather limited. This is in line with the results of Leegwater [21], who also found a narrow stability

#127287 - $15.00 USD Received 21 Apr 2010; revised 19 Jul 2010; accepted 19 Jul 2010; published 6 Aug 2010

region. However, in [21] this region was observed to become larger when the frequency dependence of the gain and absorption was taken into account. Based on these considerations, our simulations are expected to be conservative estimates of the laser properties. The results in [22] also indicate that it could be possible to tune the α-parameters by changing the bias voltage without affecting the dynamics for certain values of the voltage.

The results of simulations performed with $\alpha_g = \alpha_q$ for two different values of the second order term, $[k^{(1)}_{\omega_0}]^2/k_0 + k^{(2)}_{\omega_0}$, in Eq. (3) are shown in Fig. 10(b). The behavior of the pulse width and the TBP is observed to be highly dependent on the sign of $[k^{(1)}_{\omega_0}]^2/k_0 + k^{(2)}_{\omega_0}$. For negative values, the pulse width increases with $\alpha_g = \alpha_q$, while it decreases for positive values. This behavior agrees with the results in [16]. Fig. 10(b) also shows that when the second order term is positive, the time-bandwidth product stays relatively close to the Gaussian transform limit of 0.44 as the pulse width decreases. The black solid line in Fig. 10(b) shows that sub-picosecond pulses are achievable even with nonzero α-parameters. However, mode-locked solutions are found only for $\alpha_g = \alpha_q < 3.6$, which is why the solid lines terminate at this value. This trend becomes more pronounced as $k^{(2)}_{\omega_0}$ gets closer to the optimum value of -2.1×10^6 ps^2/km found in Fig. 9(b), where mode-locked solutions occur for $\alpha_g = \alpha_q < 1.6$. Thus, the linewidth enhancement factors limit the attainable pulse width. However, this also shows that dispersion engineering can be used to achieve mode-locking for certain values of the α-parameters, although at the price of larger pulse widths.

4. Conclusion

In conclusion, we have presented a model for a new type of photonic crystal passively mode-locked laser. The laser model predicts that a PCW laser should be capable of emitting stable, sub picosecond, and nearly transform limited pulses of high quality. Extensive numerical investigations of the interplay between the gain dynamics and the strong dispersion of the PCW show that the laser is predicted to exhibit mode locking behavior for a large range of parameter values. This fact shows promise for a realization of the type of design shown in Fig. 1. The repetition rate of the laser is shown to be tunable over a wide range by adjusting the group velocity of the pulses in the PCW inside the cavity. The proposed laser design is to the best of our knowledge the first to combine a passively mode-locked scheme with a PC slow-light structure in order to obtain very compact and highly versatile ML lasers suitable for integration on photonic chips. The conclusions have been reached with the simplifying assumption of the ring cavity model, and future work should address linear cavities featuring bidirectionally propagating fields.

Acknowledgements

The authors acknowledge financial support from Villum Fonden via the NATEC (NAnophotonics for TErabit Communications) Centre.

#127287 - $15.00 USD Received 21 Apr 2010; revised 19 Jul 2010; accepted 19 Jul 2010; published 6 Aug 2010